Journal Name

ARTICLE TYPE

Cite this: DOI: 10.1039/xxxxxxxxxx

Photocarrier Dynamics in Monolayer Phosphorene and Bulk Black Phosphorus

Peymon Zereshki,[†a] Yaqing Wei,[†b] Frank Ceballos,[a] Matthew Z. Bellus,[a] Samuel D. Lane,[a] Shudi Pan,[c] Run Long,[*b] and Hui Zhao,[*a]

Received Date
Accepted Date

DOI: 10.1039/xxxxxxxxxx

www.rsc.org/journalname

We report a combined theoretical and experimental study on photocarrier dynamics in monolayer phosphorene and bulk black phosphorus. Samples of monolayer phosphorene and bulk black phosphorus were fabricated by mechanical exfoliation, identified according to their reflective contrasts, and protected by covering them with hexagonal boron nitride layers. Photocarrier dynamics in these samples was studied by an ultrafast pump-probe technique. The photocarrier lifetime of monolayer phosphorene was found to be about 700 ps, which is about 9 times longer than bulk black phosphorus. This trend was reproduced in our calculations based on *ab initio* nonadiabtic molecular dynamics combined with time-domain density functional theory in the Kohn-Sham representation, and can be attributed to the smaller bandgap and stronger nonadiabtic coupling in bulk. The transient absorption response was also found to be dependent on the sample orientation with respect to the pump polarization, which is consistent with the previously reported anisotropic absorption of phosphorene. In addition, an oscillating component of the differential reflection signal at early probe delays was observe in the bulk sample and was attributed to the layer-breathing phonon mode with an energy of about 1 meV and a decay time of about 1.35 ps. These results provide valuable information for application of monolayer phosphorene in optoelectronics.

Two-dimensional (2D) materials beyond graphene have drawn considerable attention since the discovery of the layer-dependent bandstructure of MoS_2 in 2012. Although initial efforts have been mostly devoted to transition metal dichalcogenides[1], since 2014, black phosphorus (BP) has emerged as a promising semiconducting material for electronic and optoelectronic applications. Bulk crystals of BP have a small bandgap[2] of about 0.3 eV. However, in few-layer BP and monolayer (1L) BP, known as phosphorene, the bandgaps increase significantly with reducing the thickness[3–6]. The sizable bandgaps, which can be controlled electrically[7], and the exceptionally high charge mobilities[8] suggest that few-layer BP and phosphorene might be a good candidate for logic electronic applications. Recently, field-effect transistors with BP or phosphorene as channel materials have been demonstrated[5,9–16]. Other novel transport phenomena, such as quantum Hall effect[17,18], quantum oscillations[19], and anisotropic Dirac semimetal state[20], have also been observed.

Black phosphorus and phosphorene have also shown potential for optical applications due to its thickness-tunable optical bandgap. Recent optical measurements revealed that phosphorene, bilayer BP, and trilayer BP have optical bandgaps of 1.73, 1.15, and 0.83 eV, respectively, at 77 K[21]. Furthermore, large binding energies in these thin materials make excitons stable at elevated temperatures[22]. The optical responses of BP and phosphorene are anisotropic[21–23], adding an additional degree of freedom for device design and functionalities. Photodetectors based on BP have shown high photoresponsivity[24,25], broadband response[26,27], polarization sensitivity[27], and the potential to be integrated with silicon photonics[28]. Other optoelectronic applications, including terahertz detection[29], midinfrared electro-optic modulation[30], photovoltaic[31], and ultrafast photoswitching[32], have also been demonstrated. Application of phosphorene and few-layer BP in other type of devices has been explored, too, such

[a] *Department of Physics and Astronomy, The University of Kansas, Lawrence, Kansas 66045, United States*
[b] *College of Chemistry, Key Laboratory of Theoretical and Computational Photochemistry of Ministry of Education, Beijing Normal University, Beijing, 100875, People's Republic of China*
[c] *College of Physics, Qingdao University, Qingdao, Shandong 266071, People's Republic of China*
[†] *These authors contributed equally.*

† Electronic Supplementary Information (ESI) available: Discussion and figure to establish optical contrast of phosphorene; See DOI: 10.1039/b000000x/

as gas sensors[33] and oxygen generation[34].

For many optoelectronic applications, photocarrier dynamics plays a key role in determining the performance of materials. However, in contrast to the significant efforts summarized in the previous paragraph, studies on photocarrier dynamics in BP are rare and are limited to bulk samples. In 2015, spatially and temporally resolved transient absorption measurements revealed a 100-ps carrier lifetime, a photocarrier diffusion coefficient of 1300 cm^2 s^{-1} at room temperature, and significant anisotropic transport properties in bulk BP[35]. Similar photocarrier lifetimes, of about 80[36] and 150 ps[37], were also reported by different groups. The transient aborption technique has also been used to study density-dependence photocarrier dynamics[38] and energy relaxation[39,40] in bulk BP as well as photocarriers dynamics in BP quantum dots[41] and amorphous BP[42]. Furthermore, scanning ultrafast electron microscopy measurements with high spatial resolutions have revealed high and anisotropic photocarrier diffusion coefficients and a lifetime of about 550 ps[43].

Studies of photocarrier dynamics in 1L phosphorene is challenging since phosphorene degrades rather rapidly in air, especially under photoexcitation[44]. However, understanding photocarrier dynamics is important for application of this material in its ultimate 2D form. Here we report an ultrafast pump-probe study of photocarrier dynamics in phosphorene and its comparison with bulk BP. We obtained a photocarrier lifetime of phosphorene of about 700 ps, which is about 9 times longer than bulk BP. This trend was reproduced in our calculations based on *ab initio* nonadiabtic molecular dynamics combined with time-domain density functional theory in the Kohn-Sham representation, and can be attributed to the smaller bandgap and stronger nonadiabtic coupling in bulk. We also observed anisotropic transient absorption response of both phosphorene and bulk BP and layer-breathing phonon mode in bulk. These results provide valuable information for application of phosphorene in optoelectronics.

Mechanical exfoliation technique has been generally used to produce 1L and few-layer 2D materials from layered crystals. However, exfoliation and identification of phosphorene and few-layer BP are challenging because of the poor air stability of this material and the expected small optical contrast of phosphorene. In our study, we first established a fast identification procedure by producing a large number of thin flakes on polydimethylsiloxane (PDMS) substrates that are about 1-mm thick. This was done by cleaving a BP crystal (purchased from 2DSemiconductors) with an adhesive tape, pushing the tape against the PDMS substrate, and then peeling off the tape. Optical micrsocope images (in reflection geometry) of thin flakes produced on PDMS were immediately taken. It has been well established that for an atomically thin layer on a thick and transparent substrate, the contrast is proportional to the number of layers[45,46]. By survey a large number of thin flakes, we established that one layer of BP has a contrast of 2.8 % (see Figure S1 in ESI). Based on this, we next produced phosphorene samples for optical measurements by rapidly searching for flakes of that contrast immediately following the exfoliation. Once identified, phosphorene and bulk BP flakes were transferred to Si/SiO_2 substrates. Each flake was fully covered by a hexagonal boron nitride (h-BN) thick layer for protection. An example of the 1L phosphorene flakes is shown in Figure 2(a).

Photocarrier dynamics in phosphorene and bulk BP were studied by time-resolved pump-probe measurements in reflection geometry. The femtosecond laser system is composed of an 80-MHz passively mode-locked Ti:sapphire laser and a photonic crystal fiber. The Ti:sapphire laser produces 100-fs pulses at 750 or 800 nm. Part of this beam is used to generate a broadband pulse in the photonic crystal fiber through supercontinuum generation process. A bandpass filter with a 10-nm bandwidth is then used to select a desired wavelength component for the measurement as the pump pulse. The other part of the Ti:sapphire output is directly used as the probe pulse. The two pulses are combined by a beamsplitter and then focused to the sample from normal direction by a microscope objective lens with a numerical aperture of 0.7. The sizes of the focused spots are about 1 - 2 μm in full-width at half-maximum (FWHM). Due to the chirp from the photonic crystal and dispersion of the objective lens, the pulses at the sample are broadened to about 250 fs. The reflected probe is sent to a Si photodiode. A mechanical chopper is used to modulate the pump beam at about 2.4 KHz. A lock-in amplifier measures differential reflection, which is defined as $\Delta R/R_0 = (R - R_0)/R_0$, where R and R_0 are the reflection coefficients of the probe with and without the presence of the pump beam, respectively[47]. This quantity provides a method to monitor the density of the photocarriers injected by the pump, since the photocarriers occupy some states in the conduction and valance bands, reducing the absorption of the probe *via* the phase-space state filling effect[47]. In the low-density regime, the differential reflection is proportional to the carrier density. In the measurements, the differential reflection is measured as a function of probe delay, which is defined as the arrival time of the probe pulse with respect to the pump pulse and is controlled *via* the travel distance of the probe pulse before entering the sample. All the measurements were performed at room temperature with samples exposed to air. The h-BN layers were found to be effective in protecting the samples, as no sample degradation was observed during the course of the study.

We first studied a bulk BP sample for comparison, as shown in the lower inset of Figure 1(a). A 650-nm pump pulse with an energy fluence of about 18 μJ cm^{-2} injects photocarriers by interband absorption. An 800-nm pulse was used as the probe. The pump and probe are linearly polarized along the horizontal and vertical directions, respectively. The upper inset of Figure 1(a) shows the signal over a short time range, while the main panel is the signal over the entire range. The data was fit by $\Delta R/R_0 = A_1\exp(-t/\tau_1) + A_2\exp(-t/\tau_2) + A_p\exp(-t/\tau_p)\sin[2\pi f(t - t_0)]$, as shown by the red curves. The upper inset provides a better view of the oscillating component at early probe delays. The parameters associated with this component are $A_p = 0.40 \times 10^{-3}$, $\tau_p = 1.35$ ps, $f = 0.24$ THz, and $t_0 = 3.00$ ps. We attribute this oscillating feature to the coherent lattice vibration excited by the pump. The frequency of 0.24 THz corresponds to a phonon energy of 1.0 meV and a wavenumber of 8.0 cm^{-1}. The energy of this phonon mode is consistent with previous identified layer-breathing mode of BP[48]. It was well known that pump-injected carriers can trigger coherent lattice vibration[49]. Here, vibration of atomic layers along the normal direction causes a modulation

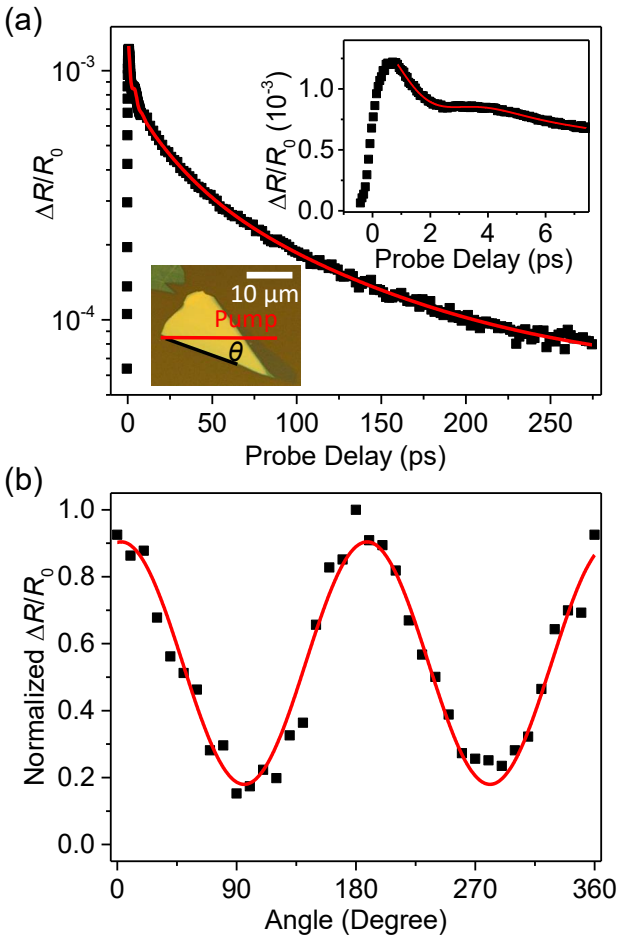

Fig. 1 (a) Differential reflection signal from the bulk BP sample shown in the lower inset. The upper inset is the signal near zero probe delay. (b) Peak differential reflection signal as a function of the sample orientation with respect to the pump polarization. The data were obtained by fixing the probe delay corresponding to the peak signal and rotating the sample about its normal direction.

of the reflection coefficient, inducing a differential reflection signal. The time constant $\tau_p = 1.35$ ps thus gives the lifetime of this mode. The first two items in the fit function dominate the signal after this transient process. The related parameters are $\tau_1 = 15$ ps, $\tau_2 = 83$ ps, and $A_2/A_1 = 1.82$. The τ_1 process could be attributed to energy relaxation of hot carriers: Since the probe photon energy of 1.55 eV is much larger than the bandgap, the probe mostly senses carriers with high energies in the conduction and valence bands. Hence, movement of carriers from the probed states to the band edge is expected to cause a decrease of the signal. However, other processes, such as trapping of carriers by defect states, could also be responsible for this decay process. We attribute the 83 ps to the photocarrier lifetime in bulk BP. This value is within the range of the previously reported photocarrier lifetimes in bulk BP by pump-probe of 80 - 150 ps[35–37]. However, it is significantly shorter than a reported value of 550 ps based on scanning ultrafast electron microscopy measurement[43]. It is unclear whether the discrepancy is due to the difference in measurement technique or sample quality.

To probe the anisotropic property of the sample, we next measured the peak differential reflection signal as a function of the angle (θ) between one edge of the flake indicated by the black line in the lower inset of Figure 1(a) and the pump polarization. The angle was varied by rotating the sample about its normal direction. The results are shown in Figure 1(b). The signal reaches a maximum when the labeled edge of the flake is parallel to the pump polarization, and follows $\cos^2(\theta)$ dependence. Both features are consistent with previous reports[35]. From these features, we can conclude that the edge is the armchair direction of the BP flake. We note that the anisotropy is quite pronounced: The signal when the armchair direction is perpendicular to the pump polarization ($\theta = 90°C$) is only about 20 % of the peak signal.

We then studied the 1L phosphorene sample shown in Figure 2(a). A 560-nm pump with an energy fluence of 28 μJ cm^{-2} injects photocarriers in the sample *via* interband absorption. We note that the change of the pump wavelength from 650 nm used in the bulk measurement is merely due to the instrumentation limit and is insignificant for the study, as both injects hot carriers with high excess energies. The carriers were probed by a 750-nm pulse. Figure 2(b) shows that the signal reaches a level of about 1×10^{-4} right after zero probe delay and then increases to about 1.2×10^{-4} in about 20 ps. The decay of the signal over the entire time range is shown in Figure 2(c), which can be fit by a single exponential function (black curve) with a decay constant of 730 ± 60 ps. It is interesting to note that the relatively slow rising of the signal is not observed in bulk BP. One possible origin of this process could be the energy relaxation of photocarriers from the states they populate right after the excitation (about 0.2 - 0.3 eV above the band edge) to the states sensed by the probe, as the probe photon energy is very close to the optical bandgap of phosphorene. In bulk, on the other hand, high-energy states were probed, and hence energy relaxation causes a decrease of the signal. However, further investigations are necessary to fully understand these features. The decay time constant can be attributed to the photocarrier lifetime in phosphorene. To confirm that the signal is not from the substrate or the *h*-BN layer, we measured the peak differential reflection signal as we scanned the pump and probe laser spots across the dashed line indicated in Figure 2(a). In this measurement, the pump fluence is 38 μJ cm^{-2}. As shown in Figure 2(d), the signal is only detectable when the laser spots are on the phosphorene area.

To probe the in-plane anisotropic properties of phosphorene, we measured the peak differential reflection signal as the sample was rotated with respect to the pump polarization. As shown in Figure 2(e), a $\cos^2(\theta)$ dependence was observed, similar to the bulk. However, the variation is only about 10 %. Previously, it has been shown that the anisotropic optical absorption of phosphorene is only pronounced for light with large excess energies. In 5-nm BP, for example, the anisotropy in absorption coefficient[23] for 560 nm light is about 10 - 20 %. The anisotropy observed here is consistent with this result and can be attributed to the anisotropy in the pump absorption. At 500 nm, however, the ratio between the absorption coefficients for light polarized along armchair and zigzag directions is as large as 3. Since bulk BP has a much smaller bandgap, the excess energy of the pump is

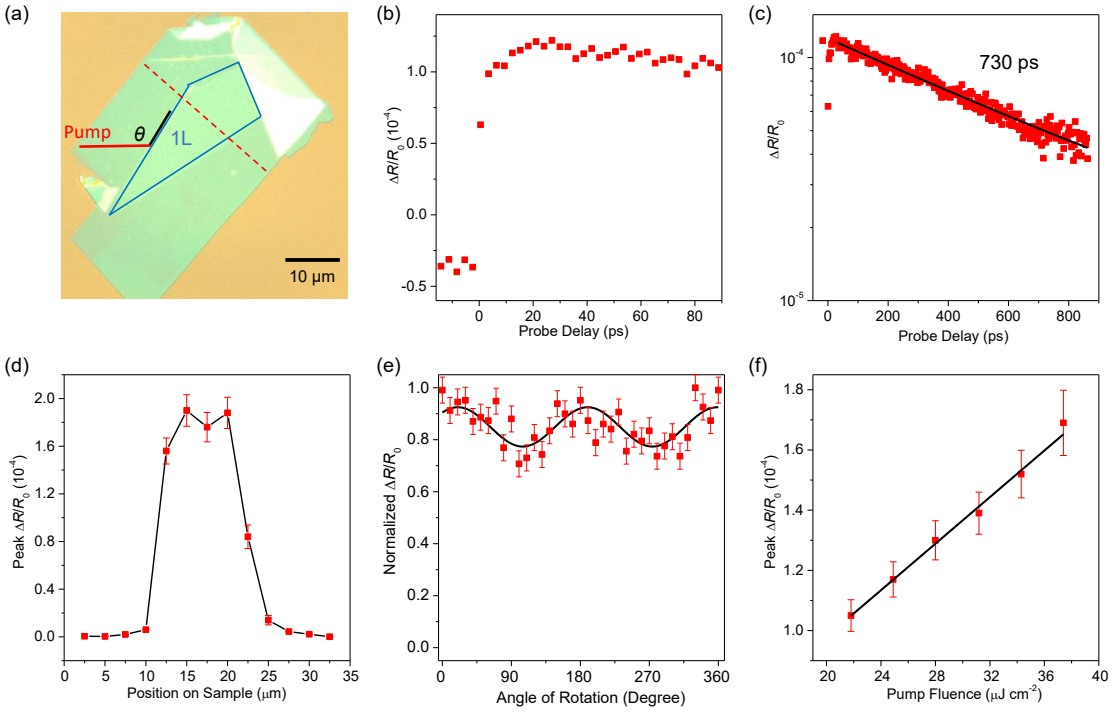

Fig. 2 (a) Monolayer phosphorene sample covered by *h*-BN. (b) Differential reflection signal from the sample in a short-time range. (c) Differential reflection signal in a long-time range. (d) Peak differential reflection signal as a function of the sample location, obtained by scanning the laser spots across the red dashed line in (a). (e) Peak differential reflection signal as a function of the sample orientation with respect to the pump polarization. (f) Peak differential reflection signal as a function of the pump fluence.

much larger for the bulk measurement, which gives rise to the large anisotropic signal shown in Figure 1(b). Finally, Figure 2(f) shows the peak signal as a function of the pump fluence. The expected linear dependence was obtained (black line), although the measurement range is limited by the poor signal-to-noise ratio and sample damage threshold. The decay time shows no apparent dependence on the pump fluence.

It is interesting that the photocarrier lifetime in 1L phosphorene is about 9 times longer than a bulk. Although both lifetimes are likely influence by defects, since they were fabricated from the same piece of BP crystal, they are expected to have similar crystalline quality. To gain more insight on the photocarrier dynamics, we applied *ab initio* nanoadiabtic (NA) molecular dynamics (MD) combined with time-domain density functional theory[50,51] in the Kohn-Sham representation[52] to model the electron-hole recombination. Both the bulk BP and the 1L phosphorene supercells contain 160 atoms. A 1.5-nm depth of vacuum slab was added along the normal of the periodic direction in 1L supercell to eliminate spurious interactions. The geometry optimization, electronic structure and adiabatic MD calculations were performed with the Vienna *ab initio* simulation package (VASP)[53]. The generalized gradient approximation functional of Perdew-Burke-Ernzerhof (PBE) functional[54] coupled with the Projected-augmented wave (PAW) method[55] was used for electronic structure calculations. The plane-wave basis energy cutoff was set as 400 eV. After the geometries were optimized at 0 K, repeated velocity rescaling was used to bring the temperature of these two systems to 300 K. Then, a 4-ps adiabatic MD simulations were performed in the microcanonical ensemble with a 1 fs atomic time-step. After that, 1000 initial system geometries were selected randomly from the 4 ps adiabatic MD trajectory to simulate the non-radiative electron-hole recombination dynamics.

To model phonon-assisted nonradiative electron-hole recombination dynamics, we utilize the classical path approximation combined with the fewest switches surface hopping (FSSH)[56]. The FSSH algorithm generates trajectory branching[56] and stratifies detailed balance[57]. Figure 3 summaries the results of the calculation on photocarrier dynamics in bulk (black) and 1L samples (red). The calculated photocarrier lifetime for bulk (22 ps) is shorter than 1L (101 ps) by about 5 times, a trend that is consistent with the experiment. We note that in both cases, the calculated lifetimes are significantly shorter than experiment. This could be attributed to the defects in realistic samples, such as vacancies, that slows electron-hole recombination[58]. For example, defects can trap one type of photocarriers, and hence prolong the lifetime of the other type. However, more investigations are needed to fully understand the discrepancy.

Photocarrier lifetime is an important parameter of semiconducting materials for optoelectronic applications. For example, longer lifetime often results in higher efficiency in photovoltaic and photodetection devices. Hence, the extended photocarrier lifetime in 1L phosphorene compared to bulk BP is encouraging for application of 1L phosphorene in optoelectronics. To understand this trend, we note that the nonradiative electron-hole re-

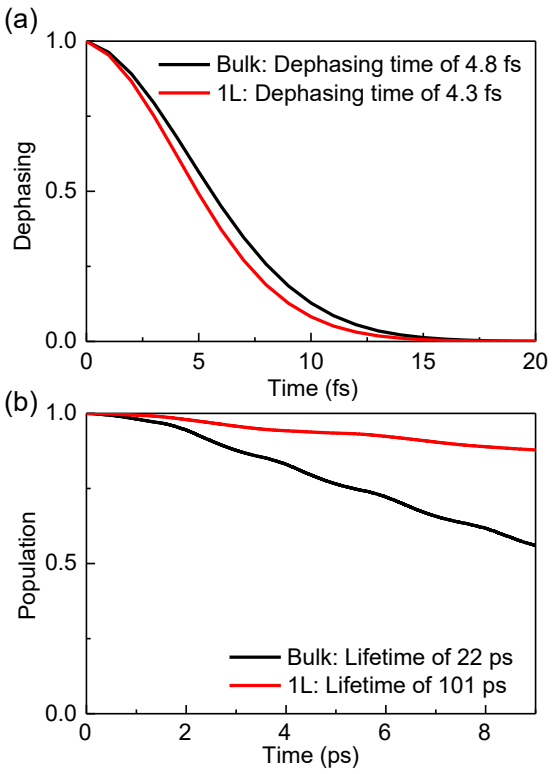

Fig. 3 (a) Pure dephasing of bulk BP (black) and 1L phosphorene (red). (b) Decay of photocarrier population in bulk BP (black) and 1L phosphorene (red).

combination rate is determined by bandgap, NA coupling, and dephasing time. Bulk BP has smaller bandgap, stronger NA coupling, and longer dephasing time than the 1L phosphorene, accelerating electron-hole recombination. In the calculation, an experimental bandgap of 0.3 eV of bulk BP[2] was used. For 1L, a 1.55 eV bandgap obtained from HSE06 calculation was adopted, since the experimental value is still rather uncertain, ranging from 1.0 to 2.0 eV[3–5]. Bulk BP has a stronger NA coupling (1.8 meV) than 1L phosphorene (0.68 meV). This arises from electron and hole wavefunctions bringing in resonances due to the small bandgap of the bulk. The dephasing time in bulk BP (4.8 fs) is slower than the 1L (4.3 fs) because interlayer interactions suppress atomic motions, which is verified by the calculated canonically averaged standard deviation of all phosphorus atoms, 0.122 versus 0.146.

In conclusion, we have studied photocarrier dynamics in monolayer phosphorene and bulk black phosphorus by transient absorption measurements. Monolayer and bulk samples were fabricated by mechanical exfoliation and protected by h-BN layers. We obtained a photocarrier lifetime of about 700 ps in monolayer phosphorene, which is about 9 times longer than the bulk sample. The extended lifetime in monolayer was reproduced in our calculations based on *ab initio* nanoadiabtic molecular dynamics combined with time-domain density functional theory in the Kohn-Sham representation. The transient absorption response was also found to be anisotropic, which is consistent with the previously reported anisotropic absorption process. Layer-breathing phonon mode with an energy of about 1 meV was observed in bulk, imposing an oscillating component to the differential reflection signal. These results provide valuable information for application of monolayer phosphorene in optoelectronics.

Acknowledgment

This material is based upon work supported by the National Science Foundation of USA (No. DMR-1505852). R. L. acknowledges the National Science Foundation of China, grant No. 21573022, and the Fundamental Research Funds for the Central Universities, grant No. 5171101561.

References

1 Q. H. Wang, K. Kalantar-Zadeh, A. Kis, J. N. Coleman and M. S. Strano, *Nat. Nanotechnol.*, 2012, **7**, 699–712.
2 D. Warschauer, *J. Appl. Phys.*, 1963, **34**, 1853–1860.
3 S. Das, W. Zhang, M. Demarteau, A. Hoffmann, M. Dubey and A. Roelofs, *Nano Lett.*, 2014, **14**, 5733–5739.
4 L. Liang, J. Wang, W. Lin, B. G. Sumpter, V. Meunier and M. Pan, *Nano Lett.*, 2014, **14**, 6400–6406.
5 H. Liu, A. T. Neal, Z. Zhu, Z. Luo, X. Xu, D. Tomanek and P. D. Ye, *ACS Nano*, 2014, **8**, 4033–4041.
6 S. Zhang, J. Yang, R. Xu, F. Wang, W. Li, M. Ghufran, Y. W. Zhang, Z. Yu, G. Zhang, Q. Qin and Y. Lu, *ACS Nano*, 2014, **8**, 9590–9596.
7 B. C. Deng, V. Tran, Y. J. Xie, H. Jiang, C. Li, Q. S. Guo, X. M. Wang, H. Tian, S. J. Koester, H. Wang, J. J. Cha, Q. F. Xia, L. Yang and F. N. Xia, *Nat. Commun.*, 2017, **8**, year.
8 J. Qiao, X. Kong, Z. X. Hu, F. Yang and W. Ji, *Nat. Commun.*, 2014, **5**, 4475.
9 Y. Du, H. Liu, Y. Deng and P. D. Ye, *ACS Nano*, 2014, **8**, 10035–10042.
10 F. Xia, H. Wang and Y. Jia, *Nat. Commun.*, 2014, **5**, 4458.
11 D. J. Perello, S. H. Chae, S. Song and Y. H. Lee, *Nat. Commun.*, 2015, **6**, 7809.
12 L. Li, Y. Yu, G. J. Ye, Q. Ge, X. Ou, H. Wu, D. Feng, X. H. Chen and Y. Zhang, *Nat. Nanotechnol.*, 2014, **9**, 372–377.
13 H. Liu, A. T. Neal, M. W. Si, Y. C. Du and P. D. Ye, *IEEE Electr. Dev. Lett.*, 2014, **35**, 795–797.
14 S. Das, M. Demarteau and A. Roelofs, *ACS Nano*, 2014, **8**, 11730–11738.
15 J. D. Wood, S. A. Wells, D. Jariwala, K. S. Chen, E. Cho, V. K. Sangwan, X. Liu, L. J. Lauhon, T. J. Marks and M. C. Hersam, *Nano Lett.*, 2014, **14**, 6964–6970.
16 H. Wang, X. Wang, F. Xia, L. Wang, H. Jiang, Q. Xia, M. L. Chin, M. Dubey and S. J. Han, *Nano Lett.*, 2014, **14**, 6424–6429.
17 L. K. Li, F. Y. Yang, G. J. Ye, Z. C. Zhang, Z. W. Zhu, W. K. Lou, X. Y. Zhou, L. Li, K. Watanabe, T. Taniguchi, K. Chang, Y. Y. Wang, X. H. Chen and Y. B. Zhang, *Nat. Nanotechnol.*, 2016, **11**, 592–596.
18 S. Tran, J. W. Yang, N. Gillgren, T. Espiritu, Y. M. Shi, K. Watanabe, T. Taniguchi, S. Moon, H. Baek, D. Smirnov, M. Bockrath, R. Y. Chen and C. N. Lau, *Sci. Adv.*, 2017, **3**, year.

19 X. Chen, Y. Wu, Z. Wu, Y. Han, S. Xu, L. Wang, W. Ye, T. Han, Y. He, Y. Cai and N. Wang, *Nat. Commun.*, 2015, **6**, 7315.

20 J. Kim, S. S. Baik, S. H. Ryu, Y. Sohn, S. Park, B. G. Park, J. Denlinger, Y. Yi, H. J. Choi and K. S. Kim, *Science*, 2015, **349**, 723–726.

21 L. K. Li, J. Kim, C. H. Jin, G. J. Ye, D. Y. Qiu, F. H. da Jornada, Z. W. Shi, L. Chen, Z. C. Zhang, F. Y. Yang, K. Watanabe, T. Taniguchi, W. Ren, S. G. Louie, X. H. Chen, Y. B. Zhang and F. Wang, *Nat. Nanotechnol.*, 2017, **12**, 21–25.

22 X. M. Wang, A. M. Jones, K. L. Seyler, V. Tran, Y. C. Jia, H. Zhao, H. Wang, L. Yang, X. D. Xu and F. N. Xia, *Nat. Nanotechnol.*, 2015, **10**, 517–521.

23 N. N. Mao, J. Y. Tang, L. M. Xie, J. X. Wu, B. W. Han, J. J. Lin, S. B. Deng, W. Ji, H. Xu, K. H. Liu, L. M. Tong and J. Zhang, *J. Am. Chem. Soc.*, 2016, **138**, 300–305.

24 M. Buscema, D. J. Groenendijk, S. I. Blanter, G. A. Steele, H. S. van der Zant and A. Castellanos-Gomez, *Nano Lett.*, 2014, **14**, 3347–3352.

25 N. Youngblood, C. Chen, S. J. Koester and M. Li, *Nat. Photo.*, 2015, **9**, 247–252.

26 M. Engel, M. Steiner and P. Avouris, *Nano Lett.*, 2014, **14**, 6414–6417.

27 H. T. Yuan, X. G. Liu, F. Afshinmanesh, W. Li, G. Xu, J. Sun, B. Lian, A. G. Curto, G. J. Ye, Y. Hikita, Z. X. Shen, S. C. Zhang, X. H. Chen, M. Brongersma, H. Y. Hwang and Y. Cui, *Nat. Nanotechnol.*, 2015, **10**, 707–713.

28 C. Chen, N. Youngblood, R. M. Peng, D. Yoo, D. A. Mohr, T. W. Johnson, S. H. Oh and M. Li, *Nano Lett.*, 2017, **17**, 985–991.

29 M. Mittendorff, R. J. Suess, E. Leong and T. E. Murphy, *Nano Lett.*, 2017, **17**, 5811–5816.

30 R. M. Peng, K. Khaliji, N. Youngblood, R. Grassi, T. Low and M. Li, *Nano Lett.*, 2017, **17**, 6315–6320.

31 M. Buscema, D. J. Groenendijk, G. A. Steele, H. S. van der Zant and A. Castellanos-Gomez, *Nat. Commun.*, 2014, **5**, 4651.

32 M. A. Huber, F. Mooshammer, M. Plankl, L. Viti, F. Sandner, L. Z. Kastner, T. Frank, J. Fabian, M. S. Vitiello, T. L. Cocker and R. Huber, *Nat. Nanotechnol.*, 2017, **12**, 207.

33 S. M. Cui, H. H. Pu, S. A. Wells, Z. H. Wen, S. Mao, J. B. Chang, M. C. Hersam and J. H. Chen, *Nat. Commun.*, 2015, **6**, year.

34 H. Wang, X. Z. Yang, W. Shao, S. C. Chen, J. F. Xie, X. D. Zhang, J. Wang and Y. Xie, *J. Am. Chem. Soc.*, 2015, **137**, 11376–11382.

35 J. He, D. He, Y. Wang, Q. Cui, M. Z. Bellus, H.-Y. Chiu and H. Zhao, *ACS Nano*, 2015, **9**, 6436–6442.

36 S. F. Ge, C. K. Li, Z. M. Zhang, C. L. Zhang, Y. D. Zhang, J. Qiu, Q. S. Wang, J. K. Liu, S. Jia, J. Feng and D. Sun, *Nano Lett.*, 2015, **15**, 4650–4656.

37 R. Z. Chen, Y. H. Tang, X. Zheng and T. Jiang, *Applied Optics*, 2016, **55**, 10307–10312.

38 R. J. Suess, M. M. Jadidi, T. E. Murphy and M. Mittendorff, *Appl. Phys. Lett.*, 2015, **107**, year.

39 K. P. Wang, B. M. Szydlowska, G. Z. Wang, X. Y. Zhang, J. J. Wang, J. J. Magan, L. Zhang, J. N. Coleman, J. Wang and W. J. Blau, *ACS Nano*, 2016, **10**, 6923–6932.

40 V. Iyer, P. D. Ye and X. F. Xu, *2D Mater.*, 2017, **4**, 021032.

41 L. Chen, C. F. Zhang, L. Li, H. Wu, X. Y. Wang, S. C. Yan, Y. Shi and M. Xiao, *J. Phys. Chem. C*, 2017, **121**, 12972–12978.

42 M. Z. Bellus, Z. B. Yang, J. H. Hao, S. P. Lau and H. Zhao, *2D Mater.*, 2017, **4**, 025063.

43 B. L. Liao, H. Zhao, E. Najafi, X. D. Yan, H. Tian, J. Tice, A. J. Minnich, H. Wang and A. H. Zewail, *Nano Lett.*, 2017, **17**, 3675–3680.

44 A. Favron, E. Gaufres, F. Fossard, A. L. Phaneuf-L'Heureux, N. Y. Tang, P. L. Levesque, A. Loiseau, R. Leonelli, S. Francoeur and R. Martel, *Nat. Mater.*, 2015, **14**, 826–832.

45 D. A. Chenet, O. B. Aslan, P. Y. Huang, C. Fan, A. M. van der Zande, T. F. Heinz and J. C. Hone, *Nano Lett.*, 2015, **15**, 5667–5672.

46 Q. Cui, R. A. Muniz, J. E. Sipe and H. Zhao, *Phys. Rev. B*, 2017, **95**, 165406.

47 F. Ceballos and H. Zhao, *Adv. Funct. Mater.*, 2017, **27**, 1604509.

48 X. Luo, X. Lu, G. K. W. Koon, A. H. C. Neto, B. Ozyilmaz, Q. H. Xiong and S. Y. Quek, *Nano Lett.*, 2015, **15**, 3931–3938.

49 L. Dworak, V. V. Matylitsky, M. Braun and J. Wachtveitl, *Phys. Rev. Lett.*, 2011, **107**, 247401.

50 X. Li, J. C. Tully, H. B. Schlegel and M. J. Frisch, *J. Chem. Phys.*, 2005, **123**, 084106.

51 S. Tretiak, K. Igumenshchev and V. Chernyak, *Phys. Rev. B*, 2005, **71**, 033201.

52 W. Kohn and L. J. Sham, *Phys. Rev.*, 1965, **140**, A1133–A1138.

53 G. Kresse and J. Furthmüller, *Phys. Rev. B*, 1996, **54**, 11169–11186.

54 J. P. Perdew, K. Burke and M. Ernzerhof, *Phys. Rev. Lett.*, 1996, **77**, 3865–3868.

55 P. E. Blöchl, *Phys. Rev. B*, 1994, **50**, 17953–17979.

56 J. C. Tully, *J. Chem. Phys.*, 1990, **93**, 1061–1071.

57 P. V. Parandekar and J. C. Tully, *J. Chem. Phys.*, 2005, **122**, 094102.

58 R. Long, W. Fang and A. V. Akimov, *J. Phys. Chem. Lett.*, 2016, **7**, 653–659.

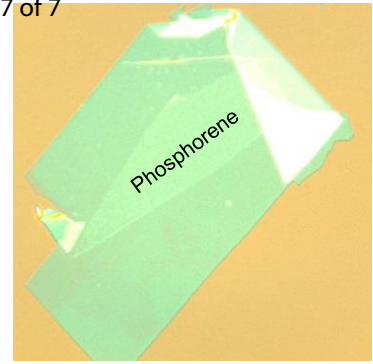

Nanoscale

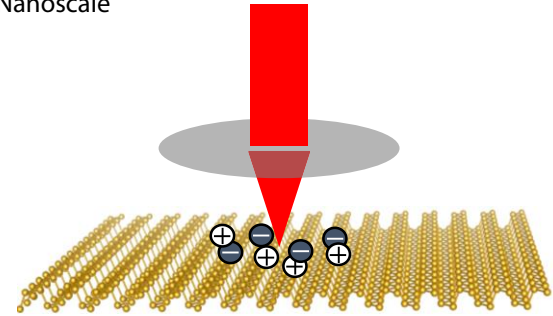

Photocarrier dynamics in phosphorene